

Real-time *In Vivo* Molecular Detection of Primary Tumors and Metastases with Ratiometric Activatable Cell-Penetrating Peptides

Elamprakash N. Savariar¹, Csilla N. Felsen¹, Nadia Nashi², Tao Jiang⁴, Lesley G. Ellies³, Paul Steinbach⁴, Roger Y. Tsien^{1,4}, and Quyen T. Nguyen²

Abstract

Management of metastatic disease is integral to cancer treatment. Evaluation of metastases often requires surgical removal of all anatomically susceptible lymph nodes for *ex vivo* pathologic examination. We report a family of novel ratiometric activatable cell-penetrating peptides, which contain Cy5 as far red fluorescent donor and Cy7 as near-infrared fluorescent acceptor. Cy5 is quenched in favor of Cy7 re-emission until the intervening linker is cut by tumor-associated matrix metalloproteinases-2 and 9 (MMP2,9) or elastases. Such cleavage increases the Cy5: Cy7 emission ratio 40-fold and triggers tissue retention of the Cy5-containing fragment. This ratiometric increase provides an accelerated and quantifiable metric to identify primary tumors and metastases to liver and lymph nodes with increased sensitivity and specificity. This technique represents a significant advance over existing nonratiometric protease sensors and sentinel lymph node detection methods, which give no information about cancer invasion. *Cancer Res*; 73(2); 855–64. ©2012 AACR.

Introduction

Cancer staging depends on evaluation of both the primary tumor and metastatic disease. In the management of many cancers such as prostate or head and neck squamous cell carcinoma (HNSCC), the extent of lymph node metastasis can often only be fully evaluated after the patient has undergone surgical removal of all anatomically susceptible lymph nodes for pathologic examination. Therefore, development of molecularly targeted imaging for more accurate detection of metastatic nodes during initial disease staging and surgery would be one of the most effective means to improve accuracy in staging and minimize morbidity associated with unnecessary lymph node dissections.

Matrix metalloproteinases (MMP) play crucial roles in cancer invasion and metastasis (1). While other MMPs are also of interest, MMP2 and 9 are currently the species with the best-established associations with tumor grade/poor prognosis and with relatively specific substrate sequences. Although MMP2,9 are also increased in inflammation/wound healing, absolute levels of these gelatinases in the head and neck have been used

to differentiate between benign papillomas versus carcinoma of the larynx (2). Increased MMP2,9 expression has been shown to correlate with cancer grade (3) and decreased survival (4, 5). In carcinoma of the tongue, increased MMP2,9 expression has been shown to correlate with incidence of lymph node metastases (6). We have previously described activatable cell-penetrating peptides (ACPP), which rely on tumor-associated MMP2,9 to unmask the adhesiveness of CPP (7, 8). Using fluorescently labeled ACPPs, we have shown improved surgical margin detection, decreased residual tumor burden, and improved survival in animal models of melanoma and breast cancer (9).

Accurate identification of whether or not a given lymph node contains cancer invasion is critical during cancer surgery. Current methods for sentinel lymph node (SLN) identification only localize the lymph node anatomically without providing any information about cancer involvement. To enable rapid molecular detection of metastatic lymph nodes during surgery, our previously described ACPPs tagged with a single fluorophore (Cy5) have been augmented with a second fluorophore (Cy7), which acts as an acceptor. Protease attack simultaneously disrupts fluorescence resonance energy transfer (FRET) and releases a highly adhesive Cy5-labeled CPP. Systemic injection of these ratiometric ACPPs (RACPP) showed MMP2,9-dependent tumor and metastatic lymph node contrast in 45 minutes and 2 hours, respectively. Ratiometric imaging represents a significant advantage over previously described single wavelength intensity measurements because it allows cancer-specific discrimination relatively independent of dose, pharmacokinetics, optical variables, and thresholding. The advantages of ratiometric versus single-intensity measurements are well known (10) in fluorescence microscopy and flow

Authors' Affiliations: ¹Department of Pharmacology, ²Division of Head and Neck Surgery, ³Department of Pathology, and ⁴Howard Hughes Medical Institute, University of California at San Diego, La Jolla, California

Note: Supplementary data for this article are available at Cancer Research Online (<http://cancerres.aacrjournals.org/>).

Corresponding Author: Quyen T. Nguyen, University of California San Diego, 9500 Gilman Drive La Jolla, CA 92093. Phone: 858-822-3965; Fax: 858-534-5270; E-mail: quyennguyen@ucsd.edu

doi: 10.1158/0008-5472.CAN-12-2969

©2012 American Association for Cancer Research.

cytometry but have hitherto been neglected in intraoperative molecular imaging. The time to develop sensitive cancer to background contrast (1–2 hours) allows intraoperative real-time assessment of lymph node status and represents a significant advance over current SLN detection methods, which identify node location without any information about cancer invasion.

Materials and Methods

Syntheses of RACPPs

Peptides were synthesized using standard solid phase Fmoc syntheses. For RACPP1, NH₂-e9-C(SS-*t*Bu)-o-PLGC(Me)AGr9cCONH₂ was reacted with Cy5 Maleimide (GE Healthcare) and subsequently treated with triethylphosphine to deprotect *tert*-BuSH group and then purified using high-performance liquid chromatography (HPLC; Note: This extra cysteine allows to covalently link solubilizing agent.) The purified compound was then reacted with SPDP-peg12-peg2-peg2-cyclo[RA₂DFK]. After completion of the reaction, Cy7mono NHS ester (Cy7-NHS, GE Health Sciences) was added to get RACPP1 (Supplementary Fig. S1a). Then, the final compound was purified using C-18 reverse-phase HPLC. Similar synthetic protocol was used to make RACPP3 (Supplementary Fig. S1d) and uncleavable control (Supplementary Fig. S1b). RACPP2 (Supplementary Fig. S2c), which lacks solubility enhancer peg12, was synthesized by reacting NH₂-e9-oPLGC(Me)AGr9cCONH₂ with Cy5-maleimide and then purified and dried. This was then reacted with Cy7-NHS to get final product and purified using HPLC. All the reactions were monitored using analytic HPLC connected with mass spectrometry (LC/MS). Characterization of final compounds using HPLC-MS indicated that the products were obtained with more than 95% purity (See Supplementary Information for details).

Generation of tumor and metastasis models

For *in vivo* imaging, we used HT-1080 xenograft in athymic nude mice or LM-P or syngeneic PyMT-derived 8119 cells in C57BL6 mice. Tumors were generated by injecting 10⁶ tumor cells into mammary fat pads of 5- to 8-week-old female mice. Animals that reached palpable tumor size typically 5 to 7 mm in size were selected for *in vivo* imaging. For the metastatic liver model, 5 × 10⁶ GFP-positive 8119 cells in PBS were injected into the spleen and allowed to circulate for 5 minutes. Vessels supplying the spleen were cauterized, the spleen removed, and wound closed. The cells circulated to the liver and were allowed to grow for 12 days. Cervical lymph node invasion with metastases from primary auricular tumors were generated as previously described (11). Briefly, GFP-labeled 8119 or 4T1 (American Type Culture Collection) mammary tumor cells were implanted (1–5 million cells) subcutaneously into the auricle of syngeneic adult wild-type mice. Cervical lymph node metastases were observed in approximately 25% to 50% of the animals by 2 to 4 weeks following subcutaneous implantation.

In vivo imaging

Animals were anesthetized using a mixture of ketamine (80 mg/kg) and midazolam (5 mg/kg); for syngeneic models, hair near the regions of interest (ROI) was removed by applying

NAIR hair remover. RACPPs or uncleavable control (9 nmoles) were intravenously injected and then animals were imaged using a whole-body mouse imager (Maestro, CRI) immediately (typically at 5 minutes), 45 minutes or 2 hours after injections unless otherwise specified. Two hours after RACPP injection, mice were euthanized by isoflurane over dose followed by cervical dislocation, and then the skin was removed and imaged using whole mouse imager (Maestro, CRI). For metastatic lymph node models, animals were injected intravenously with 10 nmoles of RACPP1 or 2 nmoles of ACPPD and imaged at 2 or 24 hours following injection, respectively.

Spectral imaging was carried out by exciting Cy5 at 620 (±10) nm followed by measuring the emission from 640 to 840 nm with 10 nm step size through a tunable LCD emission filter. Cy5 emission intensity images were obtained by exciting at 620 (±10) nm and collecting the emission light tuned to 670 nm. For ratio imaging, numerator (Cy5) and denominator (Cy7) images were synthesized by integrating spectral images over a defined range at 10 nm intervals (660–720 nm for Cy5 and 760–830 for Cy7). Ratio images were calculated, processed and color encoded using custom software. The ratio value for each pixel was encoded as hue (blue–red scale), and the brightness for each pixel was based on its corresponding brightness in the original Cy5 image. Animals with metastatic lymph node(s) were also imaged using a customized Olympus (MVX10) fluorescence ratio imaging system. ROIs were delineated using ImageJ and analyzed. Statistical analyses were conducted using 2-tailed Student *t* test. Dot density graphs were generated using Sigmaplot (12.3).

Histology

Dissected lymph nodes were immediately embedded in Tissue Tek and frozen. Cryosections (10 μm) were obtained serially at the rate of 1 section every 100 μm through the entire lymph node. Histologic analyses were conducted using hematoxylin and eosin (H&E) staining by a pathologist blinded to experimental conditions.

Characterization of RACPP cleavage

RACPP1 or RACPP2 was subjected to MMP9 (PF140, Calbiochem-EMD) cleavage in Tris buffer (50 mmol/L Tris, 10 mmol/L CaCl₂, 150 mmol/L NaCl, 0.05% Brij35, pH 7.4) for 90 minutes. The emission spectrum of uncleaved and MMP9-treated RACPP1 (400 nmol/L) in plasma was measured by exciting the Cy5 at 630 nm and collecting the emission from 640 to 840 nm in a cuvet spectrofluorometer (FluorLog, Horiba Scientific). For gel electrophoresis, MMP9-treated, untreated and urine samples were run in 10% Tricine containing PAGE (Invitrogen) in SDS-tricine buffer for 90 minutes at 100 mV and then imaged both Cy5 [λ_{ex} = 620 (±10) nm, λ_{em} = 670 nm] and Cy7 [λ_{ex} = 734 (±22) nm, λ_{em} = 820 nm] fluorescence using Maestro (CRI, Inc.) imager (Supplementary Fig. S3a and S3b). Before loading in to the well, the MMP9-treated sample was diluted 4-fold with running buffer to avoid any saturation of Cy5 emission due to dequenching. All 3 components (intact uncleaved peptide, r9 and e9 fragments) are well separated and can be seen as distinct bands in the gel (Supplementary Fig. S3a and S3b).

Results

Characterization of RACPP

The fluorescent donor and acceptor are placed on the polycationic and polyanionic domains respectively (Fig. 1A), which enforce sufficiently close proximity for FRET and synergistically combine fluorescence dequenching with preferential retention of the cleaved probe. Ratio of the donor to acceptor emissions in RACPP results in more rapid and specific tumor contrast than in previously described nonratiometric ACPPs (Fig. 1A). The emission spectrum of a prototypic RACPP (RACPP1, cleavable sequence = PLGC(Me)AG) in mouse plasma (Fig. 1B, black line) shows only slight emission from Cy5 (peak ~ 670 nm) compared with re-emission of Cy7 (peak ~ 780 nm), consistent with strong FRET. Addition of MMP9 increased Cy5 emission by about 10-fold and decreased Cy7 re-emission by about 4-fold (Fig. 1B, red dashed line). The net 40-fold increase in the ratio of 670/780 nm emissions exceeds the dynamic range of the best emission ratiometric Ca^{2+}

indicators (12) or intramolecular FRET-paired fluorescent proteins (13).

In vivo imaging using RACPP

To test tumor-dependent Cy5/Cy7 ratiometric change in living mice, we intravenously injected HT-1080 tumor-bearing *nu/nu* mice with either RACPP1 ($n = 4$) or an uncleavable control probe [cleavage sequence replaced by a poly(ethylene-glycol) linker (peg6) of equal length, $n = 4$]. Direct Cy5 fluorescence imaging of mice injected with RACPP1 (ex 620 nm, em 670 nm, Maestro, CRI at 2 hours after injection) showed higher fluorescence intensity in tumor than in normal tissues (Fig. 2A, arrow on tumor), whereas mice injected with control peptide did not (Fig. 2B). We then conducted multispectral imaging of the same mice (ex 620, em 640–840 nm), deconvoluted the spectrum at each pixel according to its dominant signature and displayed the pseudocolor assigned to that signature (Maestro software, CRI). This spectral classification

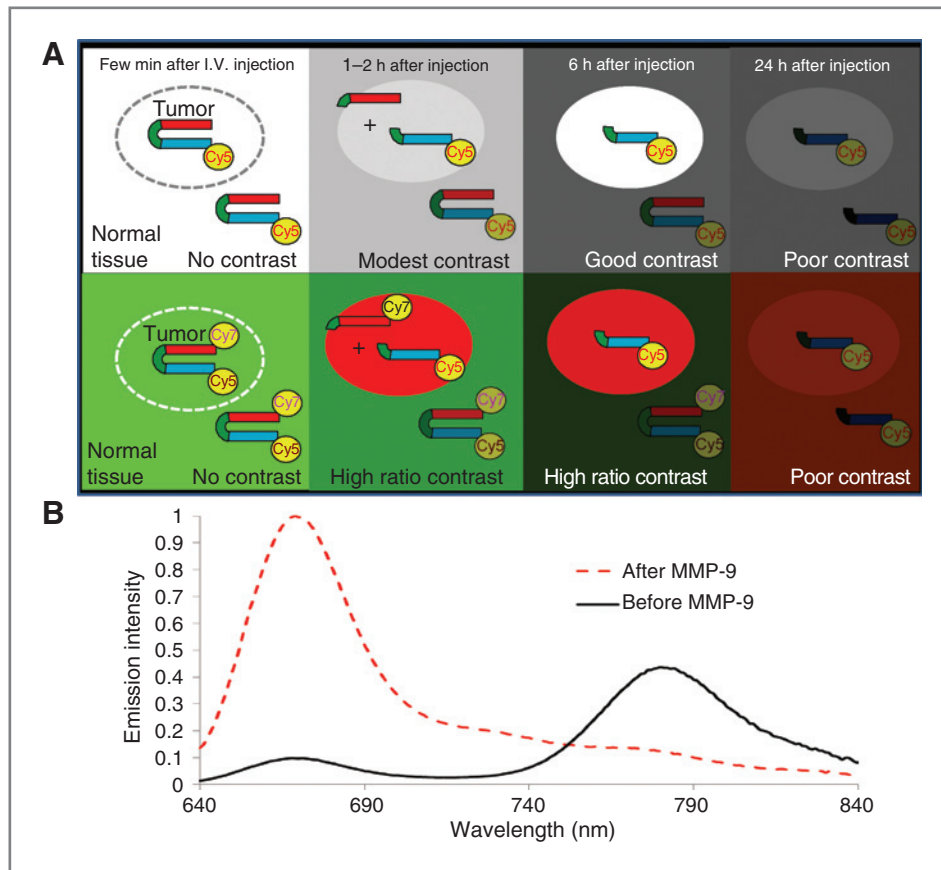


Figure 1. A, schematics of how previous nonratiometric ACPPs (standard ACPP, top) and RACPP (bottom) generate contrast for tumor (ellipse) over normal tissue. Within a few minutes after i.v. injection, neither configuration has had time to produce any tumor contrast (far left). Within 1 to 2 hours, the standard ACPP (optimal contrast at 6 hours) gives modest tumor to background contrast due to incomplete pharmacokinetic washout of the uncleaved probe from normal tissues, whereas spectacular tumor contrast can be obtained with RACPP (pseudocolor red denotes high Cy5/Cy7 emission ratio as in Figs. 2–5). Excessive waiting time such as 24 hours after i.v. injection results in loss of tumor contrast in either configuration (far right) due to eventual background cleavage in normal tissues and/or slow migration of cleavage product from sites of high enzymatic activity. B, emission spectrum of RACPP1, excited at 630 nm, measured in mouse plasma in a cuvet spectrofluorometer before (black solid curve) and after (red dashed curve) more than 95% complete cleavage with MMP-9. The starting spectrum shows considerable quenching of the Cy5 peak at 670 nm and re-emission from Cy7 at 780 nm, whereas the final spectrum is almost purely that of Cy5.

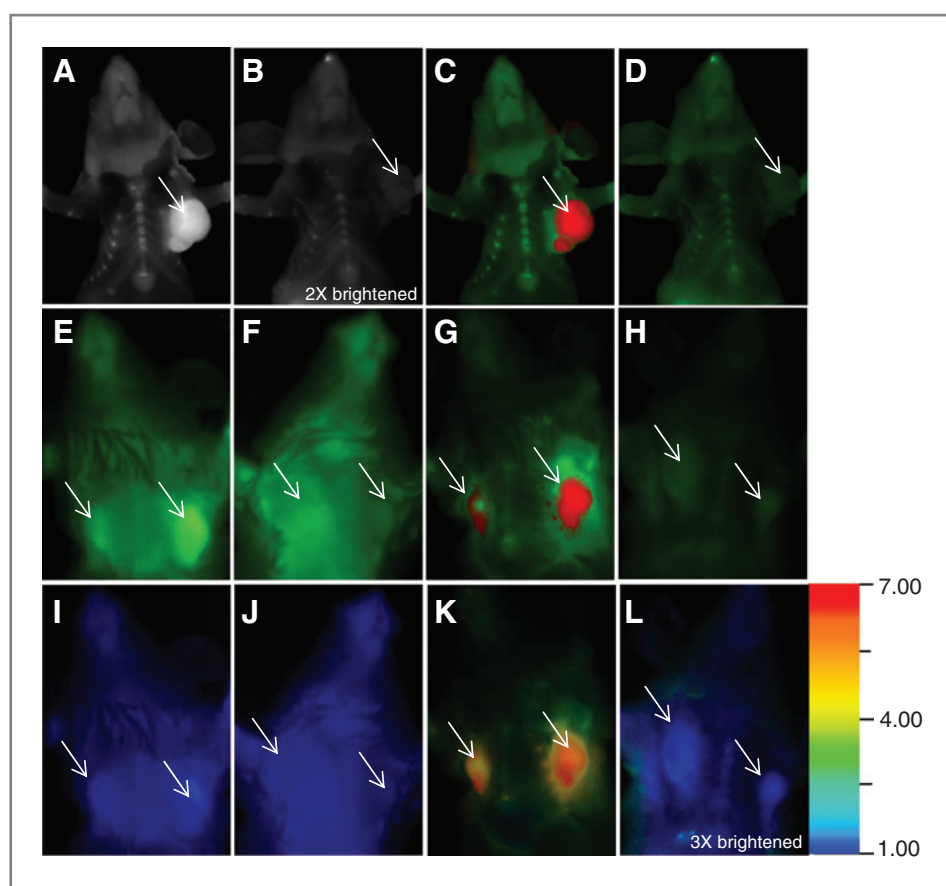


Figure 2. A and B, Cy5 intensity images (ex 620 nm, em 670 nm) 2 hours after i.v. injection of RACPP1 (A) or uncleavable control (B) into mice bearing HT-1080 xenografts after skin removal. C and D, spectrally classified imaging on the same mice where pixels with only Cy5 emission are pseudocolored red (RACPP1 cleaved), whereas pixels with both Cy5 and Cy7 emission peaks are pseudocolored green, (RACPP1 largely intact). In A, there is increased Cy5 uptake not only in the tumor (arrow) but also in the remnant skin over the head and neck region as well as the cartilage of anterior ribs. Thus, if fluorescence intensity alone were used as a measure of MMP activity, then one might deduce that there are cancer cells present in these adjacent regions as well. However, in C (spectral images), we clearly see that only the tumor (arrow) has high Cy5 intensity and low Cy7 intensity (i.e., high Cy5/Cy7 ratio, depicted in red), whereas the other regions have high Cy5 intensity and also high Cy7 intensity (i.e., low Cy5/Cy7 ratio, depicted in green). The control uncleavable probe (D) remained uncleaved in all tissues (green). White arrows indicate tumor regions. Spectrally classified (E–H) and ratiometric (I–L) imaging of mice bearing subcutaneous LM-P syngeneic grafts following i.v. injection of RACPP1 (E, G, I, K) or uncleavable control (F, H, J, L). Within 5 minutes following i.v. injection, there was a slight increase in fluorescence intensity uptake by the tumor compared with adjacent normal tissue for both probes; however, neither probe gave contrast between tumor and adjacent normal tissue in spectrally classified (E and F) or ratio (I and J) images. However, tumors showed strong spectrally classified contrast 2 hours later (G, arrows) correlating with significant Cy5/Cy7 ratio change (K) compared with adjacent normal tissue whereas control probe gave neither spectrally classified (H, arrows) nor ratio tumor contrast (L). The increase in tumor fluorescence intensity in E is likely due to additional probe molecules contained within the extra blood volume in a bulging xenograft. The tumors in F and H (obtained with uncleavable control probes) also show this similar effect. Student *t* test comparing the cleavable (E) to uncleavable probe (F) tumor Cy5/Cy7/muscle Cy5/Cy7 ratio is not significant ($P = 0.092176$). In these tumors, at the 5-minute after injection time point, lack of RACPP cleavage is shown by dominance of Cy7 spectrum (pseudocolored green), whereas at 2 hours (G), the tumor showed Cy5 spectral dominance (pseudocolored red) signifying RACPP cleavage. The lack of ratio contrast in the same tumors (I and L) shows the immunity of ratioing to such artifacts of xenografts and show the power of the ratiometric imaging.

(14) visually distinguishes the tumor, in which FRET has been disrupted (Fig. 2C, arrow on tumor, red pseudocolor), from normal tissues, in which FRET remains largely intact (green pseudocolor). The same spectral classification showed that control probe remained uncleaved in both tumor and normal tissues (Fig. 2D, arrow on tumor). Spectral classification requires computation time and discrete pseudocolors to be assigned, thus we also compared traditional displays in which increasing ratios are shown as pseudocolors smoothly varying from blue to red. When we plotted the ratio in all the obtained images, the cleavable probe gave 1.95-fold higher ratio of Cy5 to

Cy7 (Cy5/Cy7) emissions in tumor than in adjacent normal tissue (5.54 ± 0.5 vs. 2.84 ± 0.33 , $n = 5$, $P < 10^{-5}$; Supplementary Fig. S4a and S4b), whereas uncleavable control probe showed lower Cy5/Cy7 ratios that were identical between tumor and adjacent normal tissue (1.27 ± 0.07 vs. 1.26 ± 0.08 , $n = 4$; Supplementary Fig. S4c and S4d). The difference between RACPP1 and its uncleavable control was highly significant for either tumor Cy5/Cy7 emission ratio ($P < 10^{-6}$) or ratio of Cy5/Cy7 in tumor versus adjacent normal tissue ($P < 7 \times 10^{-4}$). The uncleavable control probe contains peg6 (peg) as a spacer to provide a control for both elastase and MMP cleavable probes.

RACPP1 also did well in an immunocompetent, syngeneic model of pancreatic cancer, LM-P (15), originally derived from liver metastases of transgenic pancreatic tumors. As expected, immediately (~5 minutes) following i.v. injection, there was no spectral tumor contrast (Fig. 2E and F), nor Cy5/Cy7 ratio change (Fig. 2I and J) with either probe. However, tumors showed strong contrast 2 hours later (Fig. 2G, arrows) correlating with significant Cy5/Cy7 ratio change (Fig. 2K, Cy5/Cy7 ratio in tumor = 5.7 ± 0.4 vs. adjacent tissue 3.0 ± 0.2 , $n = 3$, $P = 2 \times 10^{-8}$), whereas control probe gave neither spectrally classified tumor contrast (Fig. 2H, arrows) nor Cy5/Cy7 ratio change (Fig. 2L, ratio = 1.16 ± 0.15 in tumor vs. 1.12 ± 0.18 in adjacent tissue, $n = 2$ mice). Again, RACPP1 gave higher ratios than uncleavable control for tumor Cy5/Cy7 before ($P < 10^{-8}$) or after normalization ($P < 3 \times 10^{-5}$) against adjacent normal tissue. LM-P cells were verified by zymography to contain high MMP2,9 activity (Supplementary Fig. S4e). Varying absolute tumor probe uptake or washout of nonspecific probe (compare left and right tumors in Supplementary Fig. S4f) did not affect Cy5/Cy7 ratiometric change (Supplementary Fig. S4h). This result emphasizes the advantage of ratiometric probes over single fluorophore or dequenching probes as tumors with differing probe distribution due to varying size or vascular disturbance may have differing absolute single wavelength intensity. However, ratioing (Supplementary Fig. S4h) tends to cancel these factors, whereas protease activity has opposite effects on numerator and denominator (Supplementary Fig. S4f and S4g).

Enzyme- and tumor-specific uptake of RACPP

To test the specificity of RACPP1 for MMP2,9, we generated a syngeneic graft model ("KO") where MMP2,9 levels were genet-

ically reduced in both the tumor (mammary cell line 8119) and the host animal (MMP2^{-/-}, 9^{-/-} mice). Within 5 minutes of i.v. RACPP1 injection, negligible tumor/normal tissue spectral or ratio contrast had developed in either KO (Fig. 3A) or wild-type mice bearing the parent 8119 line with normal MMP2,9 activity (Fig. 3B). However, by 45 minutes, spectral classification revealed tumor to adjacent normal tissue contrast in WT (Fig. 3D) but not in KO (Fig. 3C). Similarly, ratiometric tumor to adjacent normal tissue contrast could be obtained only in WT (Supplementary Fig. S5d, ratio = 1.82 ± 0.14 , $n = 3$ mice), not in KO (Supplementary Fig. S5c, ratio = 1.13 ± 0.13 , $n = 3$, $P = 4 \times 10^{-5}$). The uncleavable control probe ($n = 3$ mice) did not produce spectrally classified (Supplementary Fig. S5e–S5h) or ratiometric (Supplementary Fig. S5i–S5l) tumor contrast in any mice. These results document that RACPP1 is effectively selective for MMP2,9 *in vivo*.

RACPPs have also explained the claim by van Duijnhoven and colleagues (16) that ACPP targeting of tumors is due to nonspecific cleavage in the circulation together with higher blood flow to tumors. Their main evidence was that 24 hours after injection, the biodistribution of their radiolabeled ACPPs was similar to that of just the CPP portion. We generated RACPP2 (cleavable sequence = PLGC(Me)AG), an analogue of RACPP1 closer in structure to those made by van Duijnhoven and colleagues. One to 2 hours following i.v. administration of RACPP1 or 2 in mice bearing HT-1080 or 8119 tumors, there was significant cleavage in the tumor but not adjacent normal tissues (Figs. 2C, G, and K and 3D–F), showing that cleavage was localized to the tumor. However, 24 hours after injection, what little fluorescence still left in the animal showed full cleavage in both tumor and most normal tissues (Fig. 3G and H). Analysis of RACPP2 excreted in the urine confirmed that it

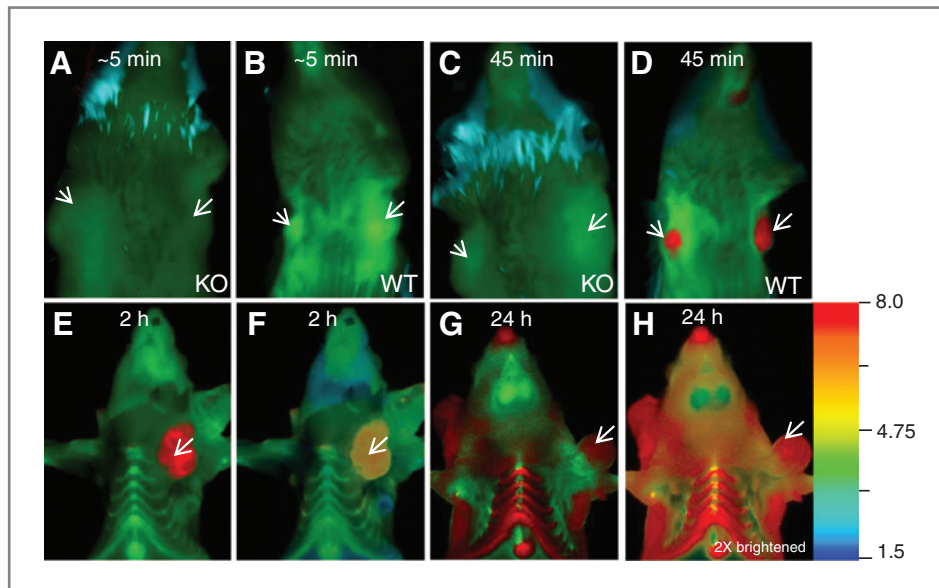


Figure 3. A–D, spectrally classified images of mice bearing syngeneic MMTV-PyMT–derived 8119 mammary tumors whose MMP2,9 levels are normal (labeled WT) or deficient (KO) following systemic i.v. RACPP1 injection. KO (A) and WT (B) mice showed high FRET about 5 minutes after injection. Significant loss of FRET was seen 45 minutes after injection in WT (C) but not in KO (D). Pseudocolor red indicates the cleaved probe and pseudocolor green indicates the uncleaved probe, whereas light blue indicates variable autofluorescence from fur. Spectrally classified (E and G) and ratio (F and H) images of mice bearing HT-1080 tumors show tumor contrast 2 hours (E and F) after i.v. injections of RACPP2, but this contrast washes out by 24 hours when most tissues only contain cleaved product (G and H).

was largely intact at 2 hours but cleaved by 24 hours (Supplementary Fig. S3a and S3b), consistent with the kinetics of *in vivo* imaging. Further evidence against initial systemic cleavage came from experiments in which the 2 precleaved halves of RACPP2 were injected. Emission ratio imaging showed complete cleavage in both tumor and normal tissues immediately (Supplementary Fig. S6a and S6e) as well as at 1 hour after injection (Supplementary Fig. S6c and S6g), quite unlike injection of intact RACPP2 (Fig. 3E and F and Supplementary Fig. S6d and S6h). Therefore, injection of RACPP2 or its cleavage products recapitulate the ambiguous results of van Duijnhoven and colleagues (16), which were observed only 24 hours after injection (see right hand panels in Fig. 1A). However the earlier images of RACPP2 prove that early cleavage is much faster in the tumor than in adjacent normal tissues or the circulation.

RACPP enable detection of metastases onto liver

Previous single fluorophore-labeled ACPPs gave high uptake into normal liver, which made it unlikely that we could distinguish metastases by standard single wavelength imaging. We have developed a syngeneic model in which GFP-labeled 8119 mammary tumor cells colonize the liver (GFP image, Fig. 4A and E). Gratifyingly, these metastases gave higher ratio contrast following RACPP1 injection than adjacent normal liver tissue (Fig. 4D). The coregistration between these ratio images and the GFP reference channel (Fig. 4A) is quite good, considering that the wavelengths for RACPP1 penetrate much more deeply than those for GFP. The 2 individual channels for Cy5 and Cy7 (Fig. 4B and C, respectively) show many coincident non-tumor accumulations (three of which are marked by arrows) that are largely canceled with ratioing. When the MMP cleavable sequence PLGC(Me)AG was replaced by an elastase-cleavable sequence, RLQLK(Ac)L (17), the resulting analogue, RACPP3, showed spectra before and after cleavage similar to those of RACPP1. This elastase probe showed an even larger difference in ratio between metastases (ratio = 5.0 ± 0.35 ,

$n = 32$ GFP-positive metastases from 4 mice) and normal liver (1.49 ± 0.1 , $P < 10^{-13}$). Ratio images of RACPP3 (Fig. 4H) again correlated much better with GFP reference images (Fig. 4E) than the constituent Cy5 and Cy7 images (Fig. 4F and G). A nonratiometric analogue of RACPP3 (17) lacking Cy7 failed to produce any contrast for liver metastases (Supplementary Fig. S7).

Detection of lymph node metastases using RACPP

To evaluate cancer involvement of individual lymph nodes (11) during surgery, mice bearing auricular primary 8119 tumors were i.v. injected with RACPP1. Within 1 to 2 hours, we found significantly increased Cy5/Cy7 ratio in lymph nodes that were invaded with cancer compared to lymph nodes that were not (Figs. 5A and Fig. 6). Mice injected to the uncleavable control RACPP showed no increased Cy5/Cy7 ratio in either metastatic or normal lymph nodes (Figs. 5B and 6A). Quantitative analysis of Cy5/Cy7 ratio change showed that RACPP was sensitive enough to detect the presence of metastatic cancer cells even when only a fraction (8%–26%) of the lymph node was invaded by cancer (Figs. 5F and H and 6A). Prospective analysis of lymph node metastases in a second set of mice with primary 4T1 tumors injected with RACPP1 using a discrimination threshold (set at ratio of 1.2 or greater) derived from the first set of 8119 lymph node metastases gave specificity = 100% ($n = 16$ of 16); sensitivity = 100% ($n = 6$ of 6).

Our previous best intensity-only probes were ACPPs attached to Cy5-labeled dendrimers (ACPPD; refs. 9, 18). We compared ACPPD and RACPP1 for their sensitivity and specificity of metastasis detection in lymph nodes following i.v. injection of either probe into mice bearing primary auricular 8119 tumors. After recording fluorescence images from the exposed nodes *in vivo*, the presence or absence of metastasis was verified by independent post mortem histology. Although the ratio of ACPPD Cy5 intensities in nodes versus adjacent normal tissue was significantly higher ($P = 0.02$) for metastatic

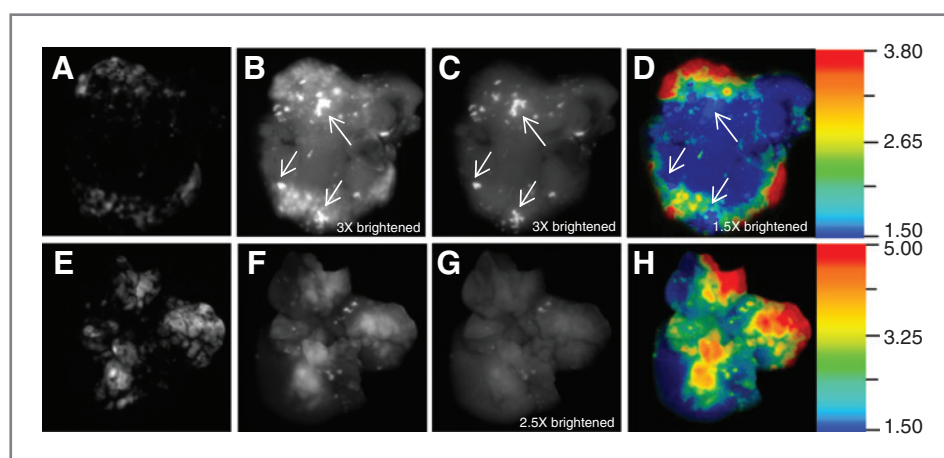
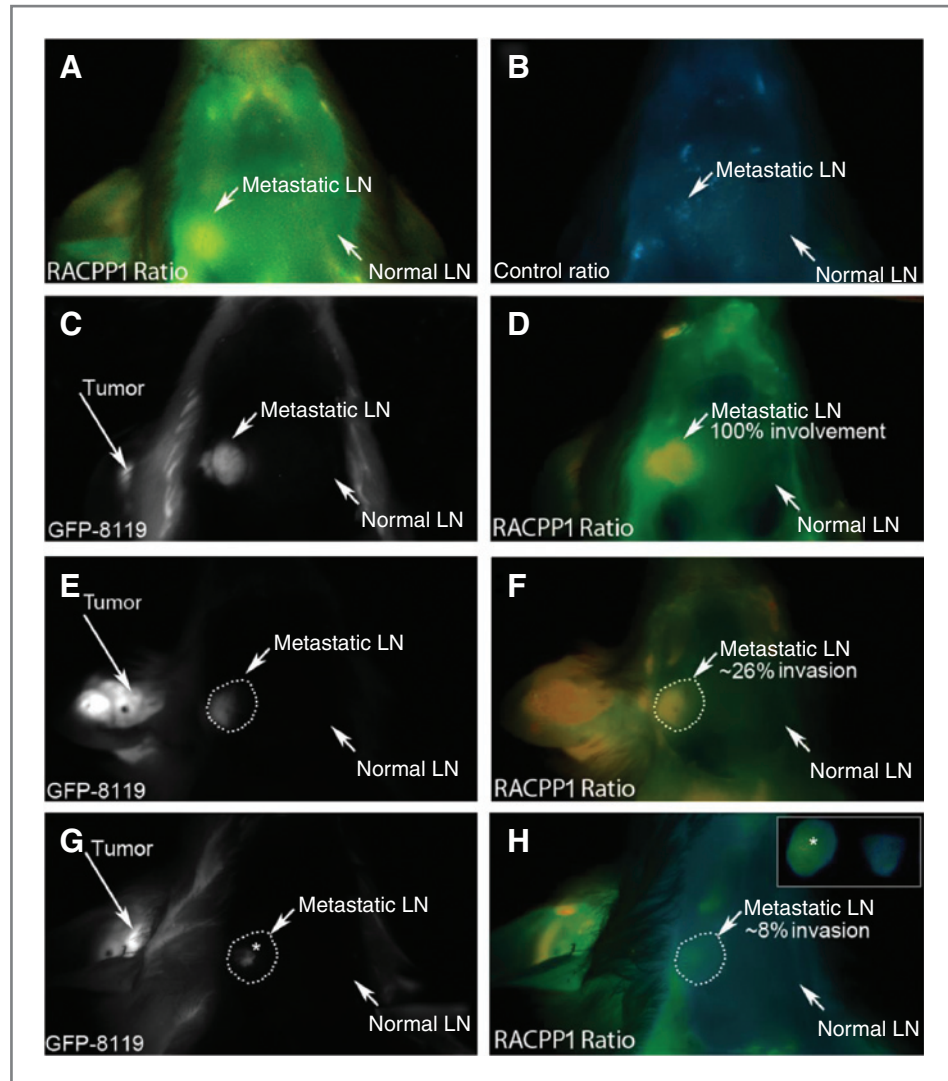


Figure 4. Livers containing PyMT 8119 GFP-positive metastases, harvested from mice 2 hours after i.v. injection of RACPP1 (MMP2,9-selective, A–D) or RACPP3 (elastase-sensitive, E–H). A and E, GFP fluorescence images. B and F, Cy5 fluorescence images obtained by exciting Cy5 at 620 nm. C and G, Cy7 emission images obtained by exciting Cy5. D and H, Cy5/Cy7 emission ratio images. Ratio images showed better correlation with GFP reference emission images than either Cy5- or Cy7-independent images. The ratio contrast for metastases relative to normal liver was higher for RACPP3 (H) than for RACPP1 (D). Arrows exemplify 2 of the many non-tumor regions (as judged by lack of GFP fluorescence) where both Cy5 and Cy7 fluorescence intensities were high, resulting in relatively low ratios.

Figure 5. Cy5/Cy7 ratiometric image of mice bearing auricular primary tumors (8119 line) showing increased ratio in pathologically confirmed metastatic lymph node (LN) but not normal LN following i.v. injection with RACPP1 (A). Mice injected with uncleavable control probe (B) did not show increased ratio in any lymph nodes. Fluorescent images of mice with primary auricular 8119 tumors bearing GFP with ipsilateral lymph node metastases (GFP images in C, E, and G) corresponding to increased Cy5/Cy7 ratio following i.v. injection with RACPP1 (D, F, and H). When there was only partial cancer invasion for a given lymph node (E and F, G and H, dotted lines showing LN contour), the area of increased ratio (F and H) localized with GFP signal (asterisk). All ratio images (A, B, D, F, H) were identically scaled over a range of 40 (minimum-maximum = 0.2–8) to accommodate the wide dynamic range provided by RACPP1. Note that although the lymph node with only 8% cancer invasion (H) had lower Cy5/Cy7 ratio in a restricted region (asterisk) compared to lymph nodes with more complete invasion (A, D, and F), ratiometric measurements still showed it to be higher than any adjacent normal tissue (insert scale narrowed to visually emphasize the ratiometric change, minimum-maximum = 2–5). H, inset, ratiometric images *ex vivo* of dissected metastatic LN and contralateral LN. See Supplementary Video S1.



than non-metastatic nodes, there was considerable overlap preventing perfect discrimination at any threshold. The same measure using only Cy5 intensities for RACPP1, that is, treating it only as a dequenching probe, gave an even more significant difference ($P = 0.0007$) and complete separation according to node status. Even more robust ($P < 10^{-4}$) discriminations of metastatic status were obtained from Cy5/Cy7 ratios of just the node or of the node further ratioed against adjacent normal tissue (Fig. 6B).

Discussion

We have developed a family of novel ratiometric probes for sensitive and specific molecular detection of primary tumors and lymph node metastases. The ratiometric pair with Cy5 as far red fluorescent donor is quenched in favor of Cy7 re-emission until the intervening linker is cleaved by tumor-associated MMP2,9 or elastases, which increase the Cy5: Cy7 emission ratio 40-fold and trigger tissue retention of the Cy5-containing fragment. This large change in ratio provides a wide

dynamic range in which protease activity in tumors and metastases can be quantitatively differentiated from adjacent normal tissue. Previous attempts to develop "smart" amplifying probes for *in vivo* imaging of protease activity have been based on fluorescence dequenching or differential pharmacokinetic washout (7, 8, 16–22). Fluorescence dequenching has been widely used because the uncleaved probe starts with low signal, which minimizes nonspecific background. These probes primarily rely on dark quenchers such as BHQ-3 or concentration-dependent self-quenching (19, 20, 23). Although these strategies have varying levels of efficacy, one inherent problem with all such methods is that fluorescence intensity is highly vulnerable to factors other than MMP activity. For example, the use of a dark quencher such as BHQ-3 has recently been shown to be problematic due to the *in vivo* instability of BHQ-3, leading to nonspecific dequenching within a few minutes after injection (24). Analogues of RACPPs have been synthesized with pheophorbide (25) or Alexa 750 (22) in place of Cy5 and BHQ-3 instead of Cy7, but these probes were nonratiometric,

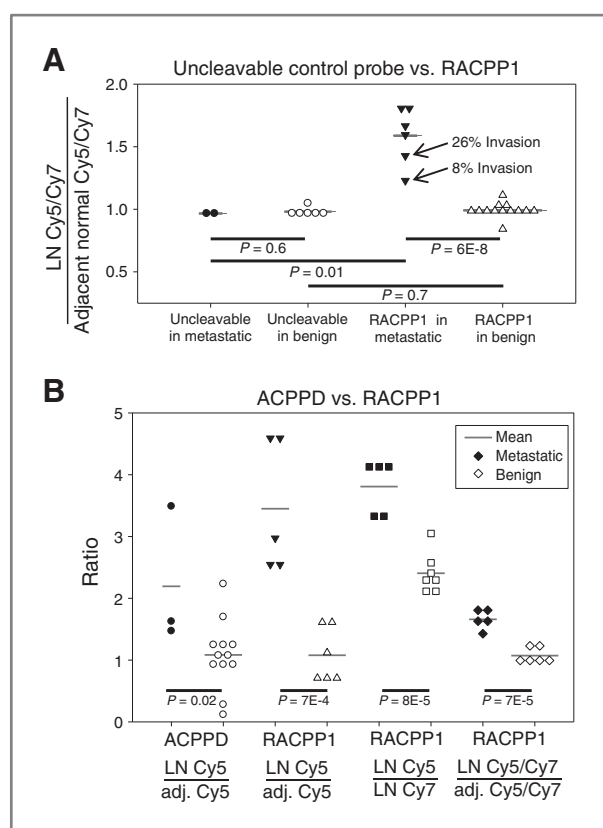


Figure 6. A, Cy5/Cy7 ratio of lymph nodes versus adjacent normal tissue in animals injected i.v. with either control uncleavable probe or RACPP1. Each symbol represents a separate lymph node whose status (solid, metastatic; hollow, non-metastatic) was independently determined by histology. In mice injected with control uncleavable probe, the presence (solid circles) or absence (hollow circles) of cancer invasion did not change the ratio of lymph node Cy5/Cy7 emission ratios relative to adjacent normal tissue, all values being near 1. In mice injected with RACPP1, lymph nodes with cancer invasion (solid triangles) had significantly higher ratios than lymph nodes without cancer invasion (hollow triangles). Interestingly, the ratio of Cy5/Cy7 emission ratios in nodes versus adjacent normal tissue correlated with the degree of cancer invasion, where the lymph nodes with partial cancer invasion (arrows) showed less ratio increase (albeit still higher than any normal tissue) than lymph nodes with 100% cancer invasion. B, dot density graph showing higher sensitivity/specificity of RACPP1 than ACPPD in the differentiation between lymph nodes bearing cancer invasion (solid symbols) versus adjacent normal tissue (hollow symbols). For ACPPD, although mean Cy5 fluorescence intensity of metastatic lymph nodes relative to adjacent normal tissue (solid circles) is significantly higher ($P = 0.02$) than for lymph nodes without metastasis (open circles), there is overlap, which decreases sensitivity/specificity. Metastatic lymph nodes in mice following i.v. injection of RACPP1 show higher Cy5 intensity relative to adjacent normal tissue (solid triangles), Cy5/Cy7 ratio alone (solid squares) or ratios against adjacent normal tissue (solid diamonds) ($P = 7 \times 10^{-4}$, 8×10^{-5} , 7×10^{-4} , respectively) than non-metastatic nodes (hollow symbols). Because metastatic and benign nodes do not overlap in the RACPP1 ratios, sensitivity and specificity can be 100%.

failed to dissociate completely after linker cleavage (perhaps because the chromophores are relatively hydrophobic and sticky), and were not tested *in vivo*. Cy5 and Cy7 both carry water-solubilizing sulfonates and a net negative charge, which probably reduce their mutual affinity and non-FRET quench-

ing. Self-quenched probes such as MMPsense are typically made from high-molecular-weight polymeric carriers that require a long post-injection wait time (24 hours; ref. 26) for optimal contrast development and washout of nonspecific binding, presumably due to the slow linker cleavage rate than small peptides. Dequenching alone cannot be differentiated from enhanced penetration and retention (EPR) or poor washout from the tumor site. Inclusion of a metabolically stable, re-emissive acceptor gives RACPPs a major advantage over previously described single fluorophore probes including our own ACPPs with or without attached dendrimers, in that the ratio of the 2 fluorescence emissions as a function of protease activity allows quantification that is independent of total probe uptake, varying washout of nonspecific binding, and thresholding (Fig. 4B–D; Supplementary Figs. S4f–S4h and S8) compared with single wavelength intensity measurements. The polycationic and polyanionic domains in RACPPs not only confer favorable pharmacokinetics (diffusible substrate before cleavage, adherent localizable product afterwards) but also maintain the approximately 40-fold increase in Cy5/Cy7 emission ratio regardless of alterations in the cleavable linker sequence. We found that RACPPs using Cy5 as fluorescent donor and Cy7 as acceptor yielded the highest ratiometric change as a function of protease activity. The Cy7 re-emission from the uncleaved probe and loss of such re-emission upon enzyme-induced probe cleavage prove that FRET is occurring. If static quenching were the dominant mechanism, there would be no sensitized Cy7 emission resulting from excitation at Cy5. Cleavage would simply amplify the donor emission spectrum without changing its wavelength distribution, as is seen with all previous far-red or NIR dequenching probes. Another prediction of a static quenching mechanism would be that the Cy7 would also be quenched in the uncleaved probe and dequenched upon cleavage. However, we have verified with direct excitation of the Cy7 that its quantum yield does not change significantly upon cleavage. Acceptors other than Cy7 tend to give more static quenching and less FRET: the ratio changes were reduced when Cy7 was replaced by CW-800, ZW-800, and Z-Cy7 (Supplementary Fig. S2). RACPPs have already been generalized to target elastases (Fig. 4E–H) and thrombin (27) and should be able to report any extracellular cleavage *in vivo* of a linker between the polycationic and polyanionic sequences.

Another important advantage of RACPP is the rapidity of ratiometric change as indicator of cancer invasion, compared with the 6- and 24-hour optimal for nonratiometric ACPPs by themselves (7, 17, 21) or attached to dendrimers (9, 18), or 24 hours for commercially available dequenching probes (26). The faster time frame (tumor to background contrast develops 1–2 hours, ratiometric imaging done in real-time by the operating surgeon) of this molecular detection method allows intraoperative real-time assessment of lymph node status and represents a significant advance to current SLN detection methods that identify node location without any information about cancer invasion. Finally, the dequenching mechanism of RACPP improved the contrast of Cy5 alone compared with single fluorophore ACPPs or ACPPD enough to enhance specificity/sensitivity for cancer detection in metastatic lymph

nodes (Fig. 6B). This interim improvement, although inferior to emission ratioing, is valuable because fluorescence imaging for clinical use (28, 29) is in its infancy and most instruments currently available in operating rooms can conduct only single fluorophore imaging. Future intraoperative implementation of RACPPs should decrease incidence of positive margins, minimize time spent waiting for a pathologist to scrutinize frozen-sectioned margins, and streamline intraoperative decision making by providing real-time knowledge of lymph node status during surgery.

Disclosure of Potential Conflicts of Interest

T. Jiang, R.Y. Tsien, and Q.T. Nguyen are scientific advisors to Avelas Biosciences, which has licensed the ACP technology from University of California Regents. No potential conflicts of interest were disclosed by the other authors.

Authors' Contributions

Conception and design: E.N. Savariar, T. Jiang, R.Y. Tsien, Q.T. Nguyen
Development of methodology: E.N. Savariar, C. Felsen, T. Jiang, L.G. Ellies, P. Steinbach, R. Tsien, Q.T. Nguyen
Acquisition of data (provided animals, acquired and managed patients, provided facilities, etc.): E.N. Savariar, C. Felsen, N. Nashi, L.G. Ellies, P. Steinbach, R.Y. Tsien, Q.T. Nguyen
Analysis and interpretation of data (e.g., statistical analysis, biostatistics, computational analysis): E.N. Savariar, C. Felsen, P. Steinbach, R.Y. Tsien, Q.T. Nguyen

Writing, review, and/or revision of the manuscript: E.N. Savariar, C. Felsen, R.Y. Tsien, Q.T. Nguyen
Administrative, technical, or material support (i.e., reporting or organizing data, constructing databases): E.N. Savariar
Developed RACPPs and conducted peptide syntheses, characterization, *in vivo* imaging: E.N. Savariar
***In vivo* imaging:** C. Felsen, N. Nashi
Developed earlier version of RACPP and synthesized ACPD: T. Jiang
Provided software support for ratio imaging: P. Steinbach
Generated MMP knockouts and liver metastasis models: L.G. Ellies

Acknowledgments

The authors thank the members of our laboratory for discussions and comments on the manuscript; K. Gibby, Q. Xiong, P. Arcaira, J. Shen, and M. Mastrodimos for technical assistance; and Dr. S. Baird for the pathologic analyses.

Grant Support

Results described here are being used in support of a patent filing by University of California San Diego. This work was supported by the Howard Hughes Medical Institute and ICMIC NCI-P50-CA128346 career development grant to E.N. Savariar, training grant 5R25CA153915 to CN Felsen, grants from the Burrough-Wellcome Fund (CAMS) and NIH (5K08EB008122) to Q.T. Nguyen, and NIH grant R01 CA158448 to R.Y. Tsien.

The costs of publication of this article were defrayed in part by the payment of page charges. This article must therefore be hereby marked *advertisement* in accordance with 18 U.S.C. Section 1734 solely to indicate this fact.

Received July 26, 2012; revised October 12, 2012; accepted November 5, 2012; published OnlineFirst November 27, 2012.

References

- Bauvois B. New facets of matrix metalloproteinases MMP-2 and MMP-9 as cell surface transducers: outside-in signaling and relationship to tumor progression. *Biochim Biophys Acta* 2012;1825:29–36.
- Uloza V, Liutkevicius V, Pangonyte D, Saferis V, Lesauskaite V. Expression of matrix metalloproteinases (MMP-2 and MMP-9) in recurrent respiratory papillomas and laryngeal carcinoma: clinical and morphological parallels. *Eur Arch Otorhinolaryngol* 2011;268:871–8.
- Wittekindt C, Jovanovic N, Guntinas-Lichius O. Expression of matrix metalloproteinase-9 (MMP-9) and blood vessel density in laryngeal squamous cell carcinomas. *Acta Otolaryngol* 2011;131:101–6.
- Liu WW, Zeng ZY, Wu QL, Hou JH, Chen YY. Overexpression of MMP-2 in laryngeal squamous cell carcinoma: a potential indicator for poor prognosis. *Otolaryngol Head Neck Surg* 2005;132:395–400.
- Mallis A, Teymoortash A, Mastronikolis NS, Werner JA, Papadas TA. MMP-2 expression in 102 patients with glottic laryngeal cancer. *Eur Arch Otorhinolaryngol* 2012;269:639–42.
- Zhou CX, Gao Y, Johnson NW, Gao J. Immunorexpression of matrix metalloproteinase-2 and matrix metalloproteinase-9 in the metastasis of squamous cell carcinoma of the human tongue. *Aust Dent J* 2010;55:385–9.
- Olson ES, Aguilera TA, Jiang T, Ellies LG, Nguyen QT, Wong E, et al. *In vivo* characterization of activatable cell penetrating peptides for targeting protease activity in cancer. *Integr Biol* 2009;1:382–93.
- Aguilera TA, Olson ES, Timmers MM, Jiang T, Tsien RY. Systemic *in vivo* distribution of activatable cell penetrating peptides is superior to cell penetrating peptides. *Integr Biol* 2009;1:371–81.
- Nguyen QT, Olson ES, Aguilera TA, Jiang T, Scadeng M, Ellies LG, et al. Surgery with molecular fluorescence imaging using activatable cell-penetrating peptides decreases residual cancer and improves survival. *Proc Natl Acad Sci U S A* 2010;107:4317–22.
- Tsien RY, Harootunian AT. Practical design criteria for a dynamic ratio imaging system. *Cell Calcium* 1990;11:93–109.
- Hoshida T, Isaka N, Hagendoorn J, di Tomaso E, Chen YL, Pytowski B, et al. Imaging steps of lymphatic metastasis reveals that vascular endothelial growth factor-C increases metastasis by increasing delivery of cancer cells to lymph nodes: Therapeutic implications. *Cancer Res* 2006;66:8065–75.
- Tsien RY. Monitoring cell calcium. In: Carafoli E, Klee C, editors. *Calcium as a cellular regulator*. New York: Oxford University Press; 1999. p. 28–54.
- Tsien RY. Indicators based on fluorescence resonance energy transfer. In: Yuste R, Konnerth A, editors. *Imaging in neuroscience and development*. Cold Spring Harbor, China: Cold Spring Harbor Laboratory Press; 2005. p. 549–56.
- Levenson R, Beechem J, McNamara G. Spectral imaging in preclinical research and clinical pathology. *Anal Cell Pathol (Amst)* 2012;35:339–61.
- Tseng WW, Winer D, Kenkel JA, Choi O, Shain AH, Pollack JR, et al. Development of an orthotopic model of invasive pancreatic cancer in an immunocompetent murine host. *Clin Cancer Res* 2010;16:3684–95.
- van Duijnhoven SM, Robillard MS, Nicolay K, Grull H. Tumor targeting of MMP-2/9 activatable cell-penetrating imaging probes is caused by tumor-independent activation. *J Nucl Med* 2011;52:279–86.
- Whitney M, Crisp JL, Olson ES, Aguilera TA, Gross LA, Ellies LG, et al. Parallel *in vivo* and *in vitro* selection using phage display identifies protease dependent tumor targeting peptides. *J Biol Chem* 2010;285:22532–41.
- Olson ES, Jiang T, Aguilera TA, Nguyen QT, Ellies LG, Scadeng M, et al. Activatable cell penetrating peptides linked to nanoparticles as dual probes for *in vivo* fluorescence and MR imaging of proteases. *Proc Natl Acad Sci U S A* 2010;107:4311–6.
- Bremer C, Bredow S, Mahmood U, Weissleder R, Tung CH. Optical imaging of matrix metalloproteinase-2 activity in tumors: feasibility study in a mouse model. *Radiology* 2001;221:523–9.
- Bremer C, Tung CH, Weissleder R. *In vivo* molecular target assessment of matrix metalloproteinase inhibition. *Nat Med* 2001;7:743–8.
- Jiang T, Olson ES, Nguyen QT, Roy M, Jennings PA, Tsien RY. Tumor imaging by means of proteolytic activation of cell-penetrating peptides. *Proc Natl Acad Sci USA* 2004;101:17867–72.

22. Levi J, Kothapalli SR, Ma TJ, Hartman K, Khuri-Yakub BT, Gambhir SS. Design, synthesis, and imaging of an activatable photoacoustic probe. *J Am Chem Soc* 2010;132:11264–9.
23. Zhu L, Xie J, Swierczewska M, Zhang F, Quan Q, Ma Y, et al. Real-time video imaging of protease expression *in vivo*. *Theranostics* 2011;1: 18–27.
24. Linder KE, Metcalfe E, Nanjappan P, Arunachalam T, Ramos K, Skedzielewski TM, et al. Synthesis, *in vitro* evaluation, and *in vivo* metabolism of fluor/quencher compounds containing IRDye 800CW and Black Hole Quencher-3 (BHQ-3). *Bioconjugate Chem* 2011;22: 1287–97.
25. Chen J, Liu TW, Lo PC, Wilson BC, Zheng G. "Zipper" molecular beacons: a generalized strategy to optimize the performance of activatable protease probes. *Bioconjugate Chem* 2009;20: 1836–42.
26. Technical Data Sheet, Fluorescent Imaging Agent MMPsense 680. Available from: www.perkinelmer.com/CMSResources/Images/44-73969TCH_NEV10126-MMPsense680-TD.pdf.
27. Whitney M, Savariar EN, Friedman B, Levin RA, Crisp JL, Glasgow H, et al. Ratiometric Activatable Cell-Penetrating Peptides Provide Rapid *In vivo* Readout of Thrombin Activation. *Angew Chem Int Ed Engl*. 2011: doi 10.1002/anie.201205721 (epub ahead of print).
28. van Dam GM, Themelis G, Crane LM, Harlaar NJ, Pleijhuis RG, Kelder W, et al. Intraoperative tumor-specific fluorescence imaging in ovarian cancer by folate receptor-alpha targeting: first in-human results. *Nat Med* 2011;17:1315–9.
29. Hutteman M, van der Vorst JR, Gaarenstroom KN, Peters AA, Mieog JS, Schaafsma BE, et al. Optimization of near-infrared fluorescent sentinel lymph node mapping for vulvar cancer. *Am J Obstet Gynecol* 2012;206:89 e1–5.